Markov Models for Directional Field and Singularity Extraction in Fingerprint Images

Sarat C. Dass*, *Member, IEEE*

Abstract— A Bayesian formulation is proposed for reliable and robust extraction of the directional field in fingerprint images using a class of spatially smooth priors. The spatial smoothness allows for robust directional field estimation in the presence of moderate noise levels. Parametric template models are suggested as candidate singularity models for singularity detection. The parametric models enable joint extraction of the directional field and the singularities in fingerprint impressions by dynamic updating of feature information. This allows for the detection of singularities that may have previously been missed, as well as better aligning the directional field around detected singularities. A criteria is presented for selecting an optimal block size to reduce the number of spurious singularity detections. The best rates of spurious detection and missed singularities given by the algorithm are 4.9% and 7.1%, respectively, based on the NIST 4 database.

Index Terms— Directional field estimation, singularity detection, Markov random field models, Bayesian statistics.

EDICS Category: 2-OTHB, 2-NFLT, 2-REST

I. Introduction

FIGURE 1 shows a fingerprint impression, of size 512×512, consisting of smoothly varying flow-like patterns (termed as ridge structures), together with important singularities (termed as cores and deltas). The direction of flow of the ridge structures at each location in the image can be represented as a two-dimensional orientation vector with unit norm. The directional field is defined as the collection of orientation vectors for all sites in the image. Singularities (cores and deltas) are points of discontinuity of the flow field. The two types of singularities are defined in terms of the ridge structures [1]; the core is the end point of the innermost curving ridge while the delta is the confluence point of three different flow directions (see Figure 1). The directional field and singularities represent two fundamental features of fingerprint impressions that need to be extracted reliably for subsequent processing [2].

Obtaining fast and reliable estimates of the directional field has been the focus of many previous research efforts; they include methods based on neural networks [3], filter-based approaches [4] and gradient-based approaches [2], [5]–[8]. However, none of these methods explicitly model the inherent spatial smoothness in the ridge structures. The detection of singularities has been addressed in many previous work. Finding regions of high curvature and subsequently classifying a feature vector into either core, delta or none of these is the approach taken in [9], [10]. In [11], geometric theory

The author is with Michigan State University, Department of Statistics & Probability, A-439 Wells Hall, E Lansing, MI 48824. E-mail: sdass@msu.edu. Phone: 517-432-5412. Fax: 517-432-1405.
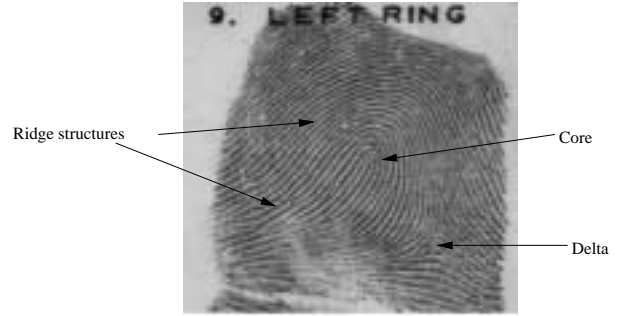

Fig. 1. Ridge structures and singularities in atypical fingerprint impression

of differential equations is used to derive signal-to-symbol representations in the flow field domain for cores and deltas. The local energy of the directional field in a neighborhood of a site is used to measure how closely it resembles a flow field around singularities in [12]. In [13], a ratio of two sines of directional fields in two adjacent regions is used to detect singularities while [2] uses a scheme for detecting singularities based on the Poincare index of the squared directional field. The present work addresses the estimation of the directional field and the detection of singularities in a Bayesian framework. A class of spatially smooth statistical models, having a Markov random field structure, is proposed as priors for the directional field. Markov random field models have been used with great success for the solution of a number of important image processing problems in which regularization based on spatial proximity is critical; these include applications in image restoration [14]–[16], segmentation [17]–[20], boundary detection [21], [22], and reconstruction in inverse problems [23], [24]. See also [25] and [26] and references therein. Other regularization techniques have also been used for image restoration (see [27] and [28], for example). The spatial smoothness induced through the Markov random field prior models restrict random variations (for example, caused by assignable noise factors such as fingertip pressure, skin elasticity and random smudges during fingerprint sensing) of directional field vectors that are spatially close, resulting in a robust extraction algorithm. Based on the robust directional field estimate, we also propose detecting singularities using parametric template models. One advantage of the parametric modelling is that a fewer number of spurious detections will be made in presence of moderate noise levels due to the restrictions placed on the directional field pattern around singularities.

In all previous work, the detection of singularities assumed

that a reliable directional field had already been extracted. One disadvantage of this approach is that the detection of a singularity does not have any impact for subsequent molding of the directional field; thus, information about singularities is not used for updating the values of the orientation vectors. We show that dynamic updating of the directional field using information on extracted singularities help detect other singularities that may have been missed previously. Our approach here will be to extract both the directional field and singularities *simultaneously* in fingerprint impressions. Thus, information on the flow field and singularities are utilized simultaneously for feature extraction resulting in improved performance. We also investigate the appropriateness of different block sizes for extracting the flow field and singularities.

II. ROBUST MODELS FOR DIRECTIONAL FIELD EXTRACTION

Several difficulties arise during the estimation of the directional field: (i) the gradient of the image intensity fluctuates in sign due to the presence of alternating ridges and furrows although the flow direction remains the same, and (ii) it is not possible to distinguish between opposite flow directions (flow at angle θ to the horizontal axis is the same as the flow along angle $\theta + \pi$). Our aim in this section is to propose models that capture the inherent spatial smoothness of the directional field while taking (i) and (ii) into account.

Consider a lattice domain $\mathcal{D} \in R^2$ consisting of r rows and c columns. An image of size $r \times c$ will be represented by its gray intensity values $I(x, y)$ for each point $(x, y) \in \mathcal{D}$. Denote by $\mathcal{C} = \{l \in R^2 : ||l|| = 1\}$ to be the unit circle in R^2. Let $\mu_s = (\frac{\partial I}{\partial x}, \frac{\partial I}{\partial y})^T$ be the (discrete) gradient vector at site $s = (x, y)$, and ν_s be the normalized version of μ_s (so that $\nu_s \in \mathcal{C}$). Let $l_s = (\cos(\theta_s), \sin(\theta_s))^T \in \mathcal{C}$ be a unit vector at site $s = (x, y) \in R^2$ representing the principal gradient direction at site s. The directional field at site s, DF_s, will be taken to be the direction orthogonal to l_s, namely

$$DF_s = l_s^\perp. \tag{1}$$

Also, let $l = \{l_s : s \in \mathcal{D}\}$, $DF = \{DF_s : s \in \mathcal{D}\}$ and $\nu = \{\nu_s : s \in \mathcal{D}\}$ denote, respectively, the site-wise principal gradient, directional field and observed gradient vectors.

For two orientation vectors l and ν in $\mathcal{C}$, the function

$$d(\nu, l) = (\nu^T l)^2 \tag{2}$$

measures the degree of similarity between two orientation vectors with $0 \le d \le 1$. The maximum (minimum) value $D = 1$ ($D = 0$) is achieved when $l = \pm\nu$ (l and ν are orthogonal to each other). Given l_s, the distribution of ν_s is given by the density

$$\pi_s(\nu_s \mid l_s) = C(\tau_s) \cdot \exp\left\{\tau_s^2 d(\nu_s, l_s)\right\}, \tag{3}$$

where $\tau_s^2 \ge 0$ is the (known) precision constant, and $C(\tau_s)$ is the appropriate normalization (independent of l_s) so that the density in (3) integrates to unity. Thus, the density in (3) is a monotonic function of the similarity measure d with modes at $\nu_s = \pm l_s$.

Assuming independence, the expression

$$\pi(\nu \mid l) = \prod_{s \in \mathcal{D}} \exp\left\{\tau_s^2 d(\nu_s, l_s)\right\} \tag{4}$$

represents the joint density (likelihood) of ν given l. In (4), we take $\tau_s^2 = \tau^2 \cdot w_s$ (with $\sum_{s=1}^N w_s = 1$), so that τ^2 represents the overall precision and each w_s measures the relative precision weights attributed to site s.

It is common in fingerprint analysis to compute a single value of the directional field for blocks of sites of size $b \times b$, say, by grouping the sites in $\mathcal{D}$. Blocking results in a spatial lattice arrangement of blocks, $\{B_{(i,j)}, 1 \le i \le r(b)$ and $1 \le j \le c(b)\}$, of size $r(b) \times c(b)$. We denote the collection of block indices in the reduced lattice arrangement, $\{(i, j) : 1 \le i \le r(b)$ and $1 \le j \le c(b)\}$, by $\mathcal{D}(b)$. Blocking assumes that the principal gradient directions l_s are constant in every block of pixels. Thus, for $u \in \mathcal{D}(b)$, we assume that $l_s = l_u$ and $w_s = w_u$ for all pixels $s \in B_u$. With blocking, the joint density (likelihood) in (4) reduces to

$$\begin{aligned}
\pi(\nu \mid l) &= \prod_{u \in \mathcal{D}(b)} \prod_{s \in B_u} \pi_s(\nu_s \mid l_u) \\
&= C_0 \prod_{u \in \mathcal{D}(b)} \exp\left\{\tau^2 w_u(l_u^T A_u l_u)\right\}, \tag{5}
\end{aligned}$$

where

$$A_u = \sum_{s \in B_u} \nu_s \nu_s^T \tag{6}$$

and w_u represents the relative precision of block B_u with respect to the rest of the blocks, and C_0 is the normalizing constant arising from the $C_0(\tau_s)$ in (4). A motivation for using the density in (5) is given in the Appendix. Also, under blocking, we have $l = \{l_u : u \in \mathcal{D}(b)\}$ and $DF = \{DF_u : u \in \mathcal{D}(b)\}$ representing the collection of block-wise principal gradient directions and directional field values, respectively.

The block-wise maximum likelihood estimate of l_u in (5) given the observed normalized gradients, ν, is given by the eigenvector corresponding to the maximum eigenvalue of A_u. Consequently, the estimated directional field corresponds to the direction orthogonal to the principal eigenvector (or, equivalently, the minimum eigenvalue of A_u). This is precisely the estimate of the directional field in [2], [5]. The relative precision weights w_u correspond to weighting the contributions of each block B_u in the joint density formula. We choose the weights

$$w_u = Coh_u \equiv \frac{\lambda_1 - \lambda_2}{\lambda_1 + \lambda_2}, \tag{7}$$

where Coh_u is the coherence measure of block B_u, and λ_1 (λ_2) is the maximum (minimum) eigenvalue of A_u. We have $0 \le Coh_u \le 1$ with $Coh_u = 1$ indicating that the gradient vectors in block B_u all point in the same direction as opposed to being uniformly distributed ($Coh_u = 0$). Thus, blocks with higher (lower) values of coherence will be more (less) favored in the overall likelihood, thus providing a strong argument for this choice of w_u.

The likelihood specified in (5) does not incorporate the spatial dependence of the principal gradient vectors (and hence, the directional field) on values in neighboring blocks.

We model the inherent spatial dependence of neighboring blocks using a Markovian prior distribution on l with a given neighborhood structure. Let $\mathcal{N} = \{\mathcal{N}_u : u \in \mathcal{D}(b)\}$ denote a neighborhood structure on $\mathcal{D}(b)$, with each $\mathcal{N}_u$ denoting the neighboring blocks of B_u. The class of spatial Markov models (indexed by α) for l is given by

$$\pi(l) = C(\alpha) \cdot \exp\left\{\lambda \sum_{u \sim v} w_{uv}\, d_\alpha(l_u, l_v)\right\}, \qquad (8)$$

where

$$d_\alpha(l, m) = |l^T m|^\alpha, \qquad (9)$$

with $\alpha > 0$ and $\lambda \geq 0$; the notation $\sum_{u \sim v}$ stands for the sum over all $u, v \in \mathcal{D}(b)$ that are neighbors of each other, w_{uv} are non-negative weights with $\sum_{v \in \mathcal{N}_u} w_{uv} = 1$, and $C(\alpha)$ is the appropriate normalizing constant. The parameter $\lambda \geq 0$ measures the degree of spatial smoothness (large (small) values of λ indicate that neighboring l values are similar (dissimilar)).

For fixed τ^2 and λ, the posterior density function of l is given by

$$\pi(l \,|\, \nu) \propto \exp\left\{\tau^2 \sum_{u \in \mathcal{D}(b)} w_u(l_u^T A_u l_u) + \lambda \sum_{u \sim v} w_{uv}\, d_\alpha(l_u, l_v)\right\} \tag{10}$$

The Maximum-a-Posteriori (MAP) estimate of l is obtained by maximizing the posterior density function in (10) with respect to l. For fixed τ^2 and λ, this is equivalent to maximizing the objective function

$$\tau^2 \sum_{u \in \mathcal{D}(b)} w_u(l_u^T A_u l_u) + \lambda \sum_{u \sim v} w_{uv}\, d_\alpha(l_u, l_v). \tag{11}$$

We describe an algorithm to find the MAP estimator of l.

The posterior distribution of l is Markovian in nature. The conditional distribution (or, local characteristics) of l_u given its neighbors l_v, $v \in \mathcal{N}_u$ is

$$\pi(l_u \,|\, l_v, v \in \mathcal{N}_u, \nu)$$
$$\propto \exp\left\{\tau^2 w_u(l_u^T A_u l_u) + \lambda \sum_{v \in \mathcal{N}_u} w_{uv} d_\alpha(l_u, l_v)\right\}. \tag{12}$$
.

We propose to maximize the posterior distribution of l in (10) using the Iterative Conditional Modes (ICM) algorithm [29], [30]. Briefly, the ICM algorithm is an iterative procedure that maximizes the conditional distribution of l_u given its neighbors and cycles through all sites $u \in \mathcal{D}(b)$ until convergence. Each update of the ICM algorithm increases the value of the posterior distribution in (10), and hence, convergence is guaranteed to a local maximum. The ICM algorithm is easily applicable in this case due to the Markovian nature of the posterior distribution of l. Starting from an initial estimate of l, l^0, the ICM algorithm updates each l_u by maximizing the local characteristic in (12) using the most current values of the remaining l_vs where $v \neq u$.

We investigate the properties of the MAP estimator for values of α ranging in $(0, 2]$. In the case when $\alpha = 2$, each conditional update entails maximizing the function

$$\tau^2 w_u(l_u^T A_u l_u) + \lambda \sum_{v \in \mathcal{N}_u} w_{uv} d(l_u, l_v) \tag{13}$$

with respect to l_u. In this case, the estimate of l_u is given by the unit eigenvector corresponding to the maximum eigenvalue of the weighted matrix

$$\frac{\tau^2 w_u}{\tau^2 w_u + \lambda} A_u + \frac{\lambda}{\tau^2 w_u + \lambda} \sum_{v \in \mathcal{N}_u} w_{uv} l_v l_v^T. \tag{14}$$

For $0 < \alpha < 2$, we find the MAP estimator of l using the optimization transfer algorithm described in [31]. The resulting algorithm is similar to the case when $\alpha = 2$ with an iterative weighing scheme $w_{uv,n}^*$ defined as

$$w_{uv,n}^* = \frac{w_{uv}}{|l_{u,n}^T l_{v,n}|^{2-\alpha}}, \tag{15}$$

to be used in (13) instead of w_{uv} at the n-th iteration. The Markovian nature of the posterior distribution enables simultaneous updates of disjoint coding sets (see [29], [30]) instead updating a single site each time. This entails significant reduction in computational time.

III. DETECTION OF SINGULARITIES

Singularities will detected based on comparing the extracted directional field (using the methodology presented in Section II) with the directional field specified by parametric template models. We use the template models for the directional field in a neighborhood around singularities as given in [2] (see Figure 2). The reason for using parametric template models is two-fold: a fewer number of spurious detections are obtained compared to non-template based methods, and parametric templates help mold the directional field values around detected singularities.

Let $\mathcal{W}_{u_0}$ denote a $w \times w$ neighborhood of sites centered at u_0. For a singular point of type $S = \{\text{core}, \text{delta}\} \equiv \{C, D\}$ centered at $u_0 = (x_0, y_0)$ and rotated ξ degrees with respect to the horizontal axis, the directional field vector at a site $u = (x, y) \in \mathcal{W}_{u_0}$ is given by

$$DF_u(S, \xi) \equiv \begin{pmatrix} \cos(\xi) & -\sin(\xi) \\ \sin(\xi) & \cos(\xi) \end{pmatrix} \cdot DF_{u^*}(S), \tag{16}$$

where $u^* = (x^*, y^*) \in \mathcal{W}_{(0,0)}$ with $x^* = (x - x_0)\cos(\xi) + (y - y_0)\sin(\xi)$ and $y^* = -(x - x_0)\sin(\xi) + (y - y_0)\cos(\xi)$,

$$DF_{u^*}(C) = \begin{pmatrix} \cos(\theta_1^*/2) \\ \sin(\theta_1^*/2) \end{pmatrix} \tag{17}$$

and

$$DF_{u^*}(D) = \begin{pmatrix} \cos(\theta_2^*/2) \\ \sin(\theta_2^*/2) \end{pmatrix}, \tag{18}$$

where (r_1^*, θ_1^*) and (r_2^*, θ_2^*) are the polar representations of $(-y^*, x^*)$ and $(-y^*, -x^*)$, respectively.

A singularity is deemed present at site u_0 if the value of the function

$$f(S, \xi; u_0) = \frac{1}{\#\mathcal{W}_{u_0}} \sum_{u \in \mathcal{W}_{u_0}} d(DF_u, DF_u(S, \xi)) \tag{19}$$

is large; in (19), DF_u is the extracted directional field vector at site u, $DF_u(S, \xi)$ is as defined in (16), $\#\mathcal{W}_{u_0}$ is the number of sites in $\mathcal{W}_{u_0}$, and d is as defined in (2). Note that in practice, the rotation angle ξ is not known and has to be estimated. We
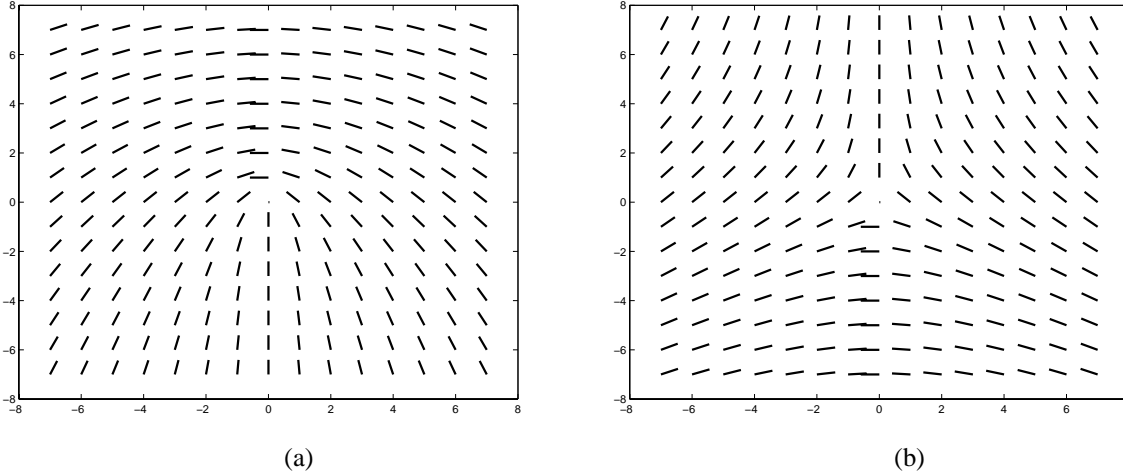
Fig. 2. The directional field for singularities based on templates: (a) core and (b) delta.

choose the estimate of ξ, $\hat{\xi}$, that maximizes $f(S, \xi; u_0)$ for each S-template model, that is,

$$\hat{\xi} = \arg \max_{\xi} f(S, \xi; u_0) \qquad (20)$$

and set

$$\hat{f}(S; u_0) = f(S, \hat{\xi}; u_0). \qquad (21)$$

The value of $\hat{f}(S; u_0)$ represents the best value of similarity of the extracted directional field with the directional field specified by the S-template model rotated at angle $\hat{\xi}$ with respect to the horizontal axis. We evaluate $\hat{f}(S; u_0)$ for all sites $u_0 \in \mathcal{D}(b)$ in a fingerprint image. The value of $\hat{\xi}$ and $\hat{f}(S; u_0)$ are obtained for each $S = \{C, D\}$. The maximum of $\hat{f}(C; u_0)$ and $\hat{f}(D; u_0)$ is then determined, and compared to a pre-specified threshold T_0 where $0 < T_0 < 1$. A singularity is said to be present at u_0 if this maximum is greater than T_0, with singularity type and orientation taken to be the ones corresponding to the maximum of $\hat{f}(C; u_0)$ and $\hat{f}(D; u_0)$. If the maximum is less than T_0, we say that no singularity is detected at u_0.

IV. SIMULTANEOUS EXTRACTION OF THE DIRECTIONAL FIELD AND SINGULARITIES

For a fingerprint image with k singularities, denote by u_i, S_i and ξ_i to be the location, type (either core or delta) and orientation of the i-th singularity, for $i = 1, 2, \ldots, k$. Singularity information for the i-th singularity is denoted by the triplet $\mathcal{S}_i \equiv (u_i, S_i, \xi_i)$, and let $\mathcal{S}(k) \equiv (\mathcal{S}_1, \mathcal{S}_2, \ldots, \mathcal{S}_k)$. We develop a joint feature extraction algorithm for the singularities and the principal gradient directions, instead of the directional field, by the equivalence in (1). Our approach will be based on an iterative scheme that comprises of the following conditional feature extraction steps: (i) extract the principal gradient directions given the information on singularities, and (ii) extract all

singularity information given the principal gradient directions. We iterate steps (i) and (ii), and terminate when no change is observed in the extracted features. An initial estimate of the principal gradient direction, l^0, followed by a singularity extraction, $\mathcal{S}(k_0)$, can be obtained using the methodology described in Sections II and III. At the n-th iteration $(n \geq 1)$, we denote the extracted principal gradient directions and the singularity information by l^n and $\mathcal{S}(k_n)$, respectively. Step (i) at the $(n+1)$-st step entails updating the values of l^n to $l^{(n+1)}$ given $\mathcal{S}(k_n)$. This is achieved conditionally by maximizing the function

$$\tau^2 \sum_{u \in \mathcal{D}(b)} w_u (l_u^T A_u l_u) + \lambda \sum_{u \sim v} w_{uv}\, d_\alpha (l_u, l_v) + \gamma \sum_{i=1}^{k_n} f(S_i, \xi_i; u_i) \qquad (22)$$

where $f(S, \xi; u)$ is as defined in (19), and $\gamma > 0$ is a pre-specified constant. The parameter γ represents the contribution of parametric directional field forms based on template singularity models to the overall objective function in (22); large values of γ indicate that the extracted directional field will closely follow the parametric forms specified by the template models. One advantage of this approach is that the detected singularities mold the directional field updates in such a way so that other singularities may be detected at subsequent iterations. We illustrate this fact in Section V. The maximization of the function in (22) can be achieved using the ICM algorithm as described in Section II. Given $l^{(n+1)}$, the singularity information is updated using the methodology presented in Section III, resulting in $\mathcal{S}(k_{n+1})$. Steps (i) and (ii) are repeated until convergence.

V. EXPERIMENTAL RESULTS

The methodology presented in the previous sections were validated on the NIST 4 fingerprint database [32]. The NIST
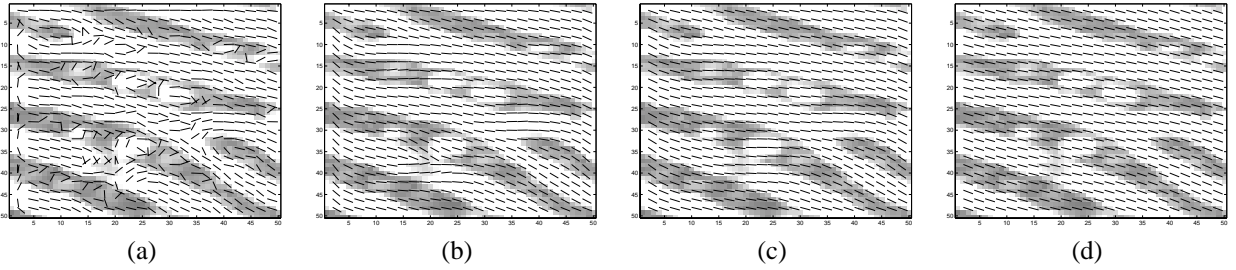
Fig. 3. Effects of λ and $\mathcal{N}_u$, (a) $\lambda = 0$, $\mathcal{N}_u$ = First Order, (b) $\lambda = 1$, $\mathcal{N}_u$ = First Order (c) $\lambda = 1$, $\mathcal{N}_u = 3 \times 3$ (d) $\lambda = 1$, $\mathcal{N}_u = 5 \times 5$. Panel (a) is Rao's estimate of the directional field that is commonly used.
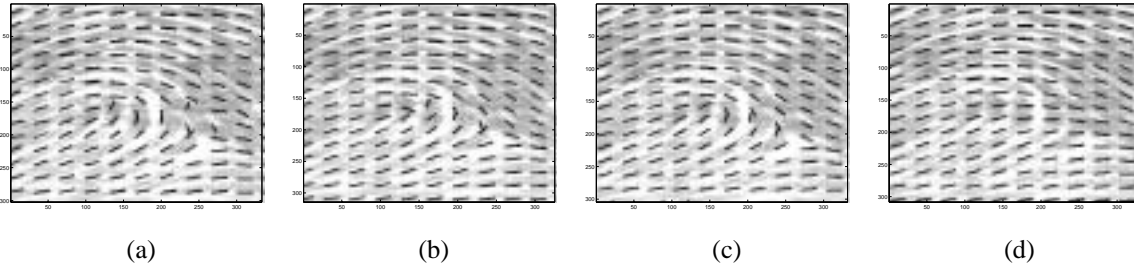

Fig. 4. Effects of increasing α and b: (a) $\alpha = 1$, $b = 5$, (b) $\alpha = 1$, $b = 10$, (c) $\alpha = 2$, $b = 5$, (d) $\alpha = 2$, $b = 10$.

4 database contains 2,000 8-bit gray scale fingerprint image pairs. Each image is 512-by-512 pixels with 32 rows of white space at the bottom and classified into one of the following five classes: arch, left-loop, right-loop, tented arch and whorl. The database is evenly distributed over each of the five classifications with 400 fingerprint pairs from each class.

A. Robust Directional Field Extraction

We investigate the performance of the directional field extraction algorithm presented in Section II. The value of τ^2 was fixed at 1 and the initial estimates of l, l^0, was taken to be the MAP estimate for $\lambda = 0$. This results in Rao's estimate of the directional field [5]. Figures 3 (a)-(d) illustrate the smoothness introduced in the directional field estimates when λ and $\mathcal{N}_u$ are increased. Three choices of $\mathcal{N}_u$ are taken: the first order (east, west, north and south neighbors), 3×3 and 5×5 neighborhood structures. A smoother and more robust directional field estimate is obtained as either λ or the neighborhood size or both are increased (compare (b)-(d) to Rao's estimate of the directional field in (a) of Figure 3). We also investigated the effect of different α values on the extracted directional field. In general, when the blocking size b is held fixed, smaller α values tend to preserve curvature information of the ridge structures compared to larger α values (see Figures 4 (a)-(d)).

B. Singularity Detection

Figure 5 illustrates the extraction of singularities in a fingerprint impression based on the methodology presented in

Section III. The directional field used to evaluate the function $\hat{f}(S; u_0)$ in (21) is obtained as in Section II, using the (3×3) neighborhood structure with $(\alpha, b) = (2, 10)$. The window $\mathcal{W}_{u_0}$ is taken to be a 11×11 neighborhood around u_0, and T_0 is taken to be 0.85. Figure III (a) shows the original fingerprint impression with two singularities (core and delta at (row,column) = (230,300) and (370,390), respectively). Applying $\hat{f}(S; u_0)$ successively for each point u_0 in the image results in a smooth surface with local maximums whose locations correspond to detected singularities of type S (see Figures III (c) and (d)). Thresholding results in a spatial clustering of points whose centers correspond to locations of singularities. Separate hierarchical clustering for $S = \{C, D\}$ is performed to determine the center of each cluster as the location of the singular points. Figure III (b) shows the extracted core and delta with estimated orientation angles -28.3^o and -0.48^o, respectively, with respect to the horizontal axis.

C. Simultaneous directional field and singularity extraction

Obtaining directional field and singularity information simultaneously offers the additional advantage of dynamic updating of features. The directional field can be dynamically molded based on current singularity information to detect other singularities in the fingerprint impression. We present two examples here to illustrate the performance improvement of the joint feature extraction algorithm compared to extraction of the directional field followed by singularity detection. Figure 6 (a) gives the results when the directional field is estimated first followed by singularity detection. The singularities are
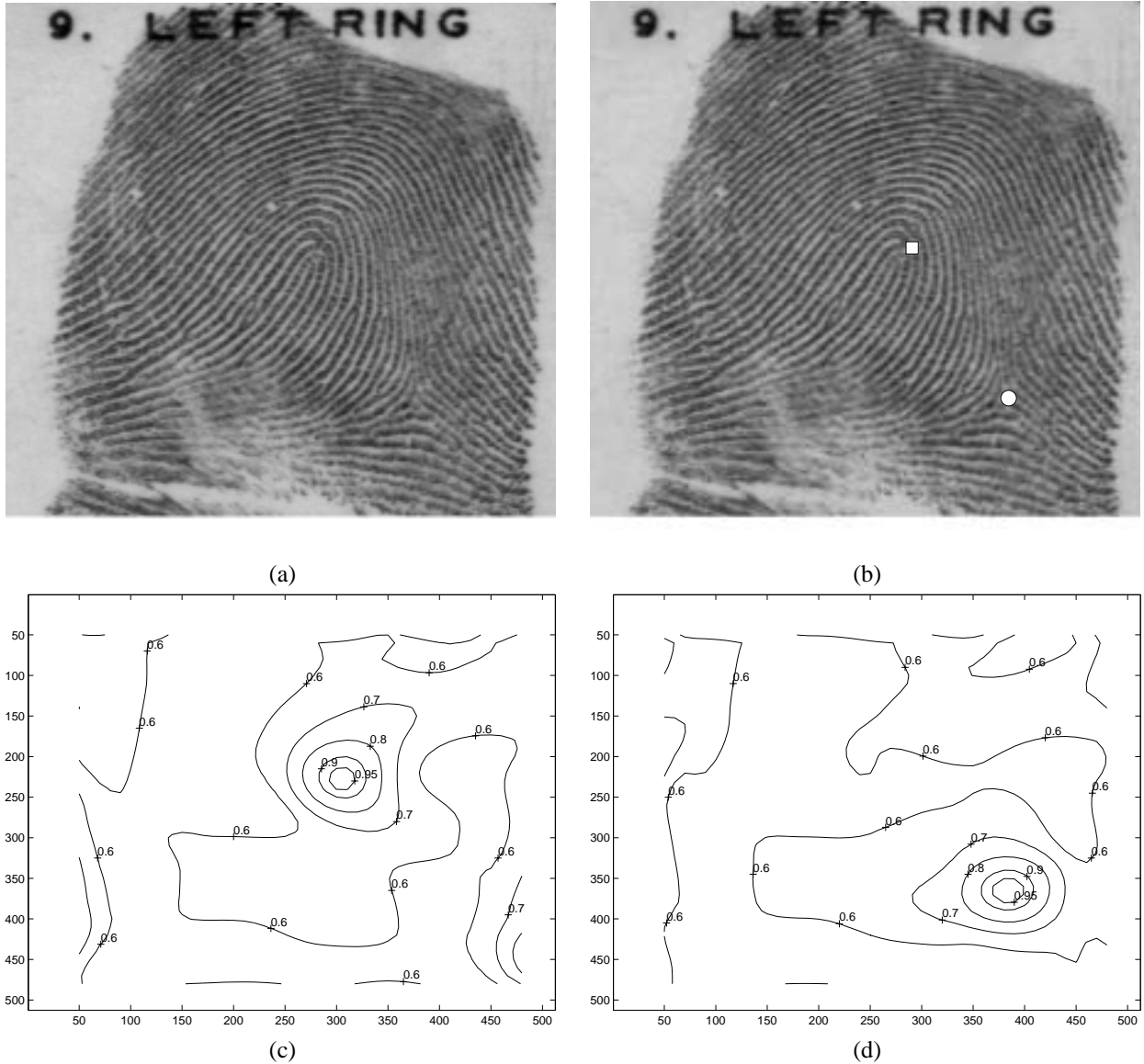
(a)

(b)

(c)

(d)

Fig. 5. Detection of singularities in fingerprint images based on template models: (a) Original image, (b) Detected singularities ($\square$ represents a core and $\circ$ represents a delta), (c) contour map of $\hat{f}(C; \cdot)$, and (d) contour map of $\hat{f}(D; \cdot)$.

detected using the filters $f(S; \cdot)$ with T_0 fixed at 0.86. Note that one core point (at (row,column) = (180,290)) is missed. Figure 6 (b) shows the detected singularities based on simultaneous directional field and singularity extraction (Section IV) using the directional field and singularity information of Figure 6 (a) as the initial estimates (l^0 and $\mathcal{S}(k_0)$, respectively). Table I (second column) gives the value of $\hat{f}(C; (180, 290))$ for 3 successive iterations, with the missed core successfully detected after the first iteration.

The singularities in Figures 6 (c) and (d) were detected using a different threshold, $T_0 = 0.96$. Note that the core at (row,column) = (250,260) is missed when joint extraction is not performed (Figure 6 (c)). Figure 6 (d) shows all singularities that are successfully detected when using the joint feature extraction algorithm. Note the increase in $\hat{f}(C; (250, 260))$ above T_0 after the first iteration in Table I (third column).

TABLE I

TABLE SHOWING THE INCREASE IN THE CORE FILTER $\hat{f}(C; \cdot)$ VALUES

Iteration	$\hat{f}(C; (180, 290))$	$\hat{f}(C; (250, 260))$
1	0.8314	0.9587
2	0.8825	0.9689
3	0.9184	0.9836

D. Effect of the blocking size, b

Figure 8 give examples of joint feature extraction based on different block sizes b. Values of b that are small cause spurious patterns to appear (see top rows of Figures 7 and 8) while large b values large (bottom rows of Figures 7 and 8) level out important ridge singularity information. Therefore, it is important to select a block size for optimal extraction of features for each fingerprint image. We present a criteria for selecting the optimal block size based on similarity measures
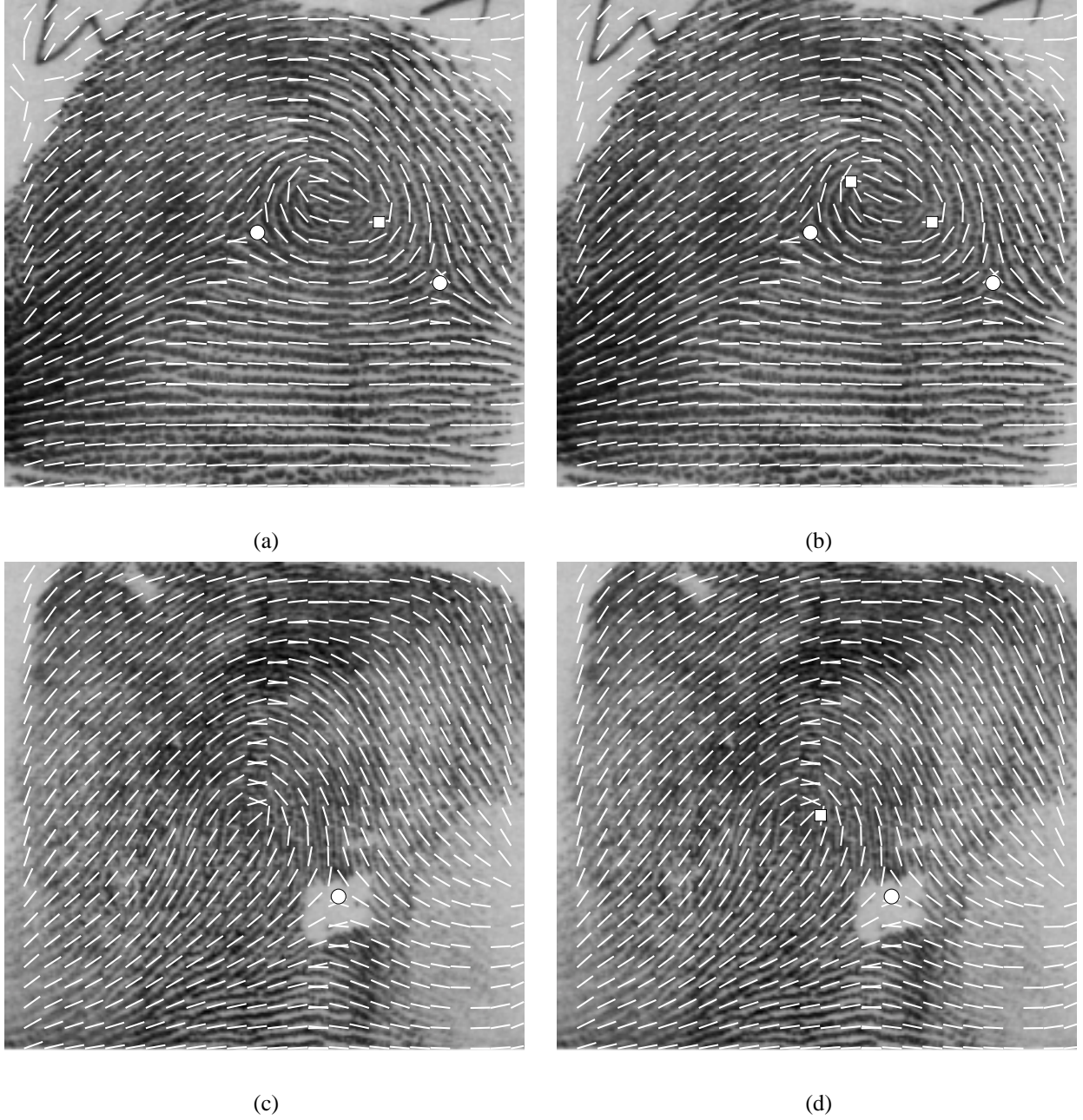
Fig. 6. A comparison of feature extraction based on two methods: one step directional field extraction followed by singularity detection ((a) and (c)), and iterative updating of the directional field and singularities ((b) and (d)).

of the extracted directional field with the true image gradients at singularity locations as well as at pre-specified locations in the fingerprint image. Denoting the locations of singularities by $u_1, u_2, \ldots, u_k$ (for k detected singularities) and the location of M pre-specified points on the fingerprint image by $r_1, r_2, \ldots, r_M$, the similarity measure with block sizes $b \times b$ is given by

$$Sim(b) = Sim_1(b) + Sim_2(b) - R_1 \cdot k - R_2 \cdot b, \quad (23)$$

where

$$Sim_1(b) = \frac{1}{k} \sum_{i=1}^{k} a_i \frac{1}{\#\mathcal{W}_{u_i}} \sum_{u \in \mathcal{W}_{u_i}} \sum_{s \in B_u} d(l_u, \nu_s) \quad (24)$$

and

$$Sim_2(b) = \frac{1}{M} \sum_{j=1}^{M} b_j \frac{1}{\#\mathcal{W}_{r_j}} \sum_{u \in \mathcal{W}_{r_j}} \sum_{s \in B_u} d(l_u, \nu_s), \quad (25)$$

where $R_1, R_2 > 0$ are constants representing the penalty terms for spurious detection and oversmoothing, respectively, $a_i, i = 1, 2, \ldots, k$ and $b_j, j = 1, 2, \ldots, M$ are pre-determined weights, and all other symbols are as described before. The optimal block size b_{opt} is chosen to maximize (23).

We applied our procedure to 1000 images from the NIST 4 database. Nine choices of b were made, namely, $b = 5, 6, 8, 10, 12, 14, 16, 18, 20$, and the criteria in (23) was evaluated to find b_{opt} for each fingerprint image. A total of $M = 25$
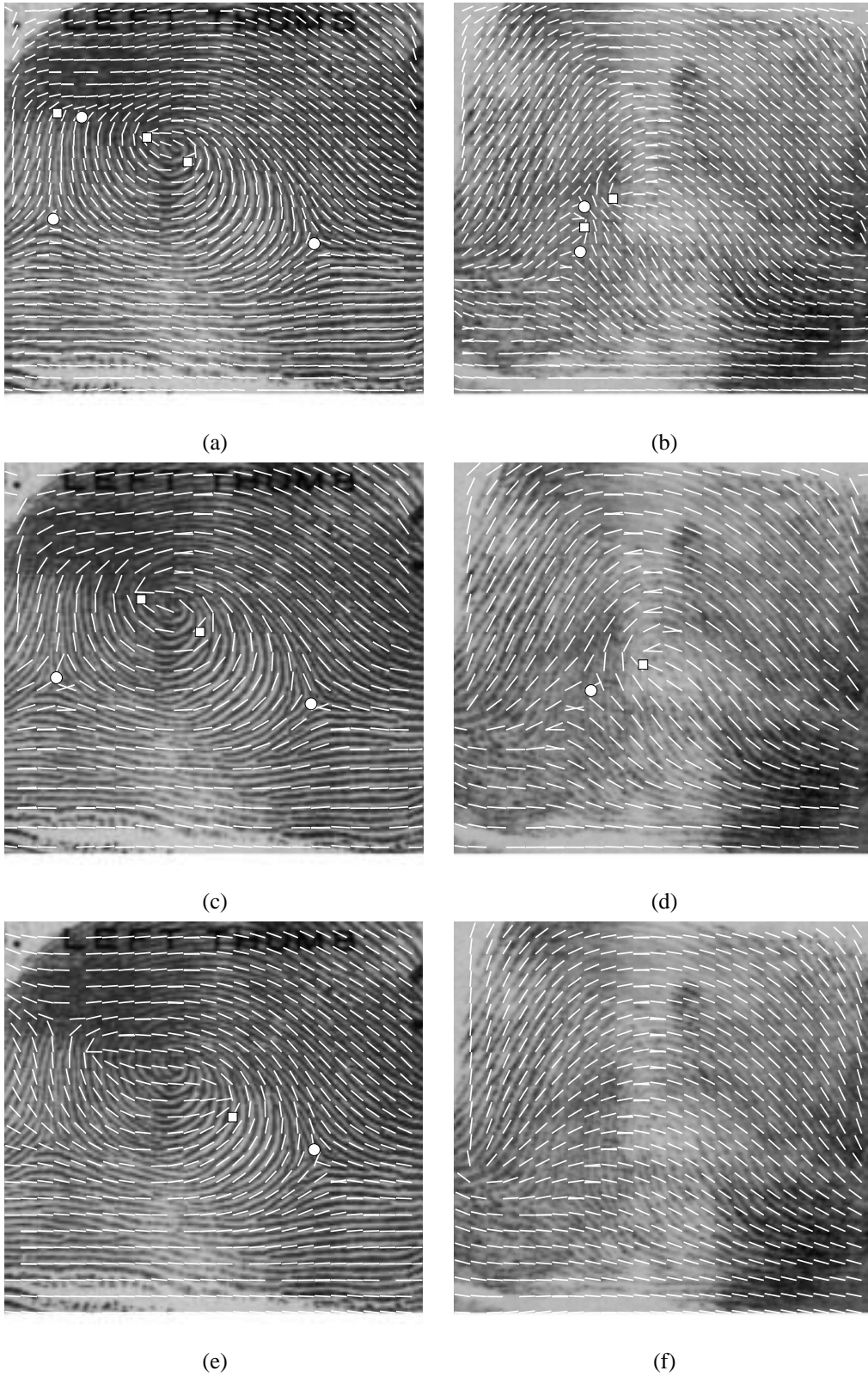
Fig. 7. Extraction of the directional field and singularities with different block sizes. Top, middle and bottom rows correspond to block sizes of 5, b_{opt} and 20, respectively. The symbols □ and ○ represents detected cores and deltas, respectively.
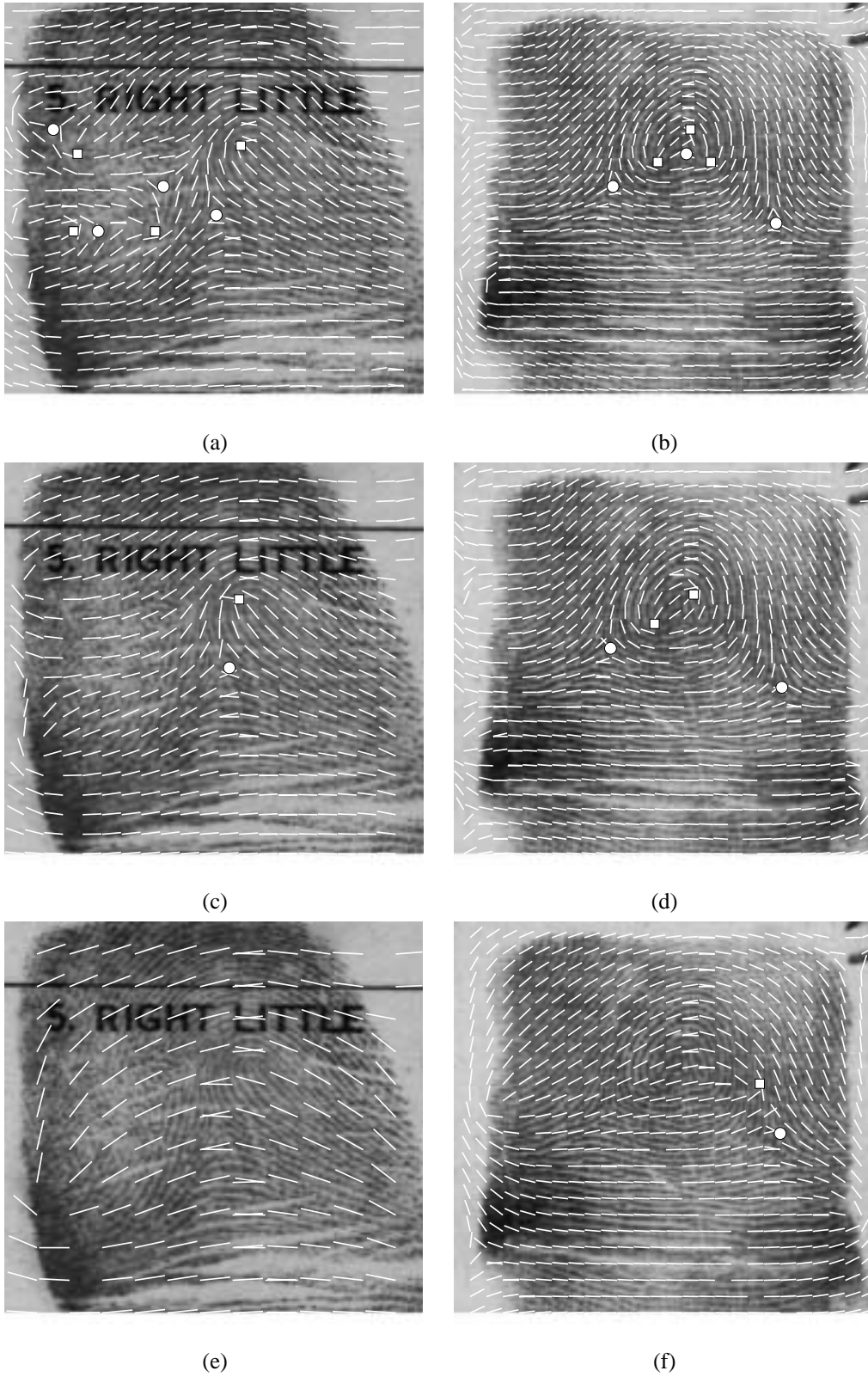
(a)

(b)

(c)

(d)

(e)

(f)

Fig. 8.   Extraction of the directional field and singularities with different block sizes. Top, middle and bottom rows correspond to block sizes of 5, b_{opt} and 20, respectively. The symbols $\square$ and $\circ$ represents detected cores and deltas, respectively.

TABLE II
AVERAGE NUMBER OF SPURIOUS DETECTIONS AND MISSED
SINGULARITIES PER FINGERPRINT IMPRESSION.

Blocking size b	Spurious detection	Missed singularities
5	0.364	0.019
b_{opt}	0.049	0.071
20	0.025	0.430

equally spaced points were chosen in the central portion of the fingerprint image. These constituted the pre-specified points b_j for $j = 1, 2, \ldots, M$. We took $R_1 = R_2 = 1$, $a_i = 2.5$ for $i = 1, 2, \ldots, k$ and $b_j = 100$ for $i = 1, 2, \ldots, M$, giving more weight to the fit at the pre-specified locations. Middle rows of Figures 7 and 8 show examples of the extracted directional field and singularities based on b_{opt}. Several spurious singularities were detected outside of the fingerprint image. We performed a manual segmentation and recorded the number of spurious and missed singularities within each fingerprint impression for $b = 5, b_{opt}$ and 20. The results are presented in Table II. The rate of spurious detection is significantly reduced when using b_{opt} although the rate of missed singularities is increased slightly. Note that the rates of spurious detection based on manual segmentation presented here is significantly lower compared to those reported in [2]

Figure 9 presents the results of simultaneous directional field and singularity extraction for 5 fingerprint classes [1] based on b_{opt}. The figures illustrate the robust extraction of the directional field and the associated singularity detection in the presence of noise. Note the robust estimation of the directional field and detection of singularities at regions with white patches in Figures 9 (a) and (c) particularly.

VI. CONCLUSION

A class of spatially smooth models are proposed for the robust extraction of the directional field, and parametric template models are used for singularity extraction. Joint extraction of the directional field and singularities has the advantage of dynamic updating of features, and the ability to detect previously missed singularities. A criteria is presented to select an optimal block size for feature extraction on an image-by-image basis. The resulting algorithm is shown to satisfactorily extract the directional field and singularities in a variety of fingerprints involving moderate noise levels.

APPENDIX I
A MOTIVATION FOR THE LIKELIHOOD MODELS OF l

In case of blocking with block sizes $b \times b$, the likelihood term for the observed normalized gradients in block B_u, $\nu^* = \{\nu_s, : s \in B_u\}$ is given by

$$
\begin{aligned}
\pi(\nu^* \mid l_u) &= \prod_{s \in B_u} C(\tau^2 w_u) \prod_{s \in B_u} \exp\{\tau^2 w_u (\nu_s^T l_u)^2\} \\
&= (C(\tau^2 w_u))^{b^2} \exp\{\tau^2 w_u \sum_{s \in B_u} (\nu_s^T l_u)^2\}
\end{aligned}
$$

A single block B_u contains alternating ridge and valley structures which cause the gradient vectors to fluctuate in sign.

Suppose that $\nu_s = e_s v$ with $\|v\| = 1$ and $e_s = \pm 1$ for $s \in B_u$. Thus, we assume that the ridge structures have one common underlying principal gradient direction (and hence one value of the directional field) but the sign of the gradients fluctuates due to the presence of alternating ridges and valleys. We have

$$
\sum_{s \in B_u} (\nu_s^T l_u)^2 = \sum_{s \in B_u} (\nu_s^T l_u)^2 = \sum_{s \in B_u} (e_s \cdot v^T l_u)^2 \leq b^2
$$

with equality if and only if $l_u = \pm v$. Thus, the maximum likelihood estimate of l_u, $\hat{l}_u = \pm v$, is independent of the sign fluctuations, e_s. Also, note that $\hat{l}_u$ is unique up to the sign of v only. In other words, $\hat{l}_u$ does not distinguish between ridge directions that are opposite to each other. It follows that each $l_u = (\cos(\theta_u), \sin(\theta_u))^T$ is uniquely determined for $\theta_u \in [-\pi/2, \pi/2]$. The same result would hold true if the function d in (2) is replaced by the more general function d_α in (9). Also, the posterior of l given the observed gradients is a function of d and d_α, and hence neighboring but opposite l directions will reinforce each other, instead of cancelling each other out.

APPENDIX II
FINDING $\hat{f}(S; u_0)$ USING A LEAST SQUARES CRITERIA

For two directional field vectors at site u, $DF_u^{(i)} = (\cos\theta_u^{(i)}, \sin\theta_u^{(i)})^T$, the squared directional field (SDF) vector is defined as

$$
SDF_u^{(i)} = (\cos 2\theta_u^{(i)}, \sin 2\theta_u^{(i)})^T = (a_u^{(i)}, b_u^{(i)})^T, \quad (26)
$$

say, for $i = 1, 2$. The closeness of the two directional field vectors can be measured using the d function in (2); we have

$$
\begin{aligned}
d(DF_u^{(1)}, DF_u^{(2)}) &= \cos^2(\theta_u^{(1)} - \theta_u^{(2)}) \\
&= 1 - \frac{(a_u^{(1)} - a_u^{(2)})^2 + (b_u^{(1)} - b_u^{(2)})^2}{4}, \quad (27)
\end{aligned}
$$

from the identity $\cos^2 \theta = (\cos 2\theta + 1)/2$ and (26). In other words, the closeness of the two directional fields can also be measured in terms of the closeness of the SDF vectors.

In order to detect a singularity at u_0, we compare the SDF values in a neighborhood of sites $u \in \mathcal{W}_{u_0}$ with that of the template models. For $S = \{C, D\}$, the ξ rotated SDF template at a point $u = u_0 + (r_u \cos\theta_u, r_u \sin\theta_u)^T$ are given by

$$
SDF_u(C, \xi) = (-\sin(\theta_u + \xi), \cos(\theta_u + \xi))^T \quad (28)
$$

and

$$
SDF_u(D, \xi) = (-\sin(\theta_u - 3\xi), -\cos(\theta_u - 3\xi))^T, \quad (29)
$$

respectively. Denote the extracted directional field and the corresponding SDF at site u by $DF_{u,ext} = (\cos(\theta_{u,ext}), \sin(\theta_{u,ext}))^T$ and $SDF_{u,ext} = (\cos(2\theta_{u,ext}), \sin(2\theta_{u,ext}))^T = (a_{u,ext}, b_{u,ext})$, respectively. To determine if a core is present at u_0, we measure the closeness of the extracted SDF with that of the template core model (28) using the least squares criteria

$$
\begin{aligned}
g(\xi; u_0) &\equiv \frac{1}{\#\mathcal{W}_{u_0}} \sum_{u \in \mathcal{W}_{u_0}} \{(a_{u,ext} + \sin(\theta_u + \xi))^2 \\
&\quad + (b_{u,ext} - \cos(\theta_u + \xi))^2\}. \quad (30)
\end{aligned}
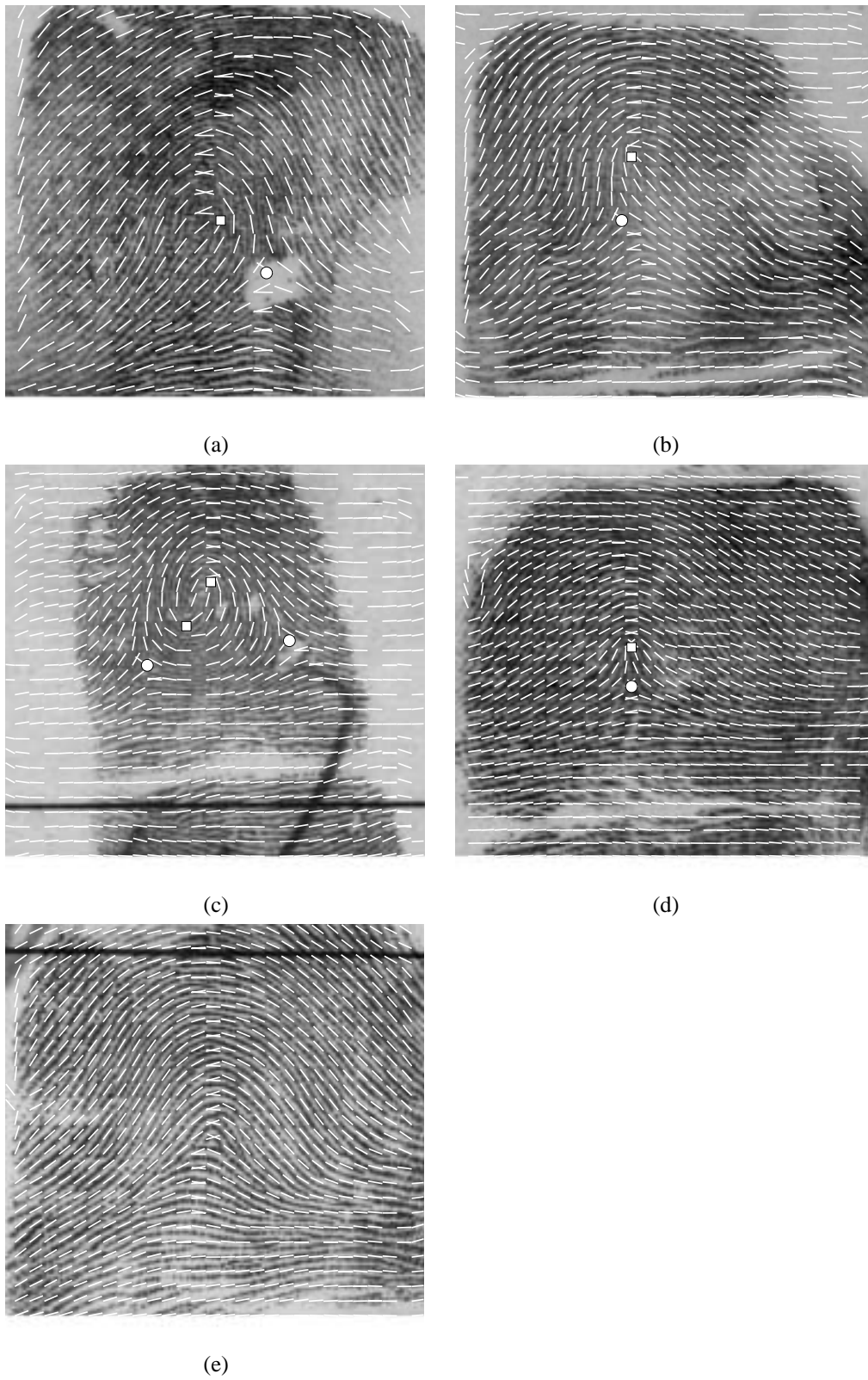$$

(a)

(b)

(c)

(d)

(e)

Fig. 9.   Robust extraction of the directional field and singularities for noisy fingerprint impressions for the 5 fingerprint classes: (a) left loop, (b) right loop, (c) whorl, (d) tented arch and (e) arch (fingerprints of class arch do not have any cores and deltas).

In (30), the rotation angle ξ is unknown and can be chosen as the value that minimizes (30) with respect to ξ. The solution $\hat{\xi}$ is given by

$$\tan \hat{\xi} = \frac{\sum_{u \in \mathcal{W}_{u_0}} (a_{u,ext}\cos(\theta_u) + b_{u,ext}\sin(\theta_u))}{\sum_{u \in \mathcal{W}_{u_0}} (a_{u,ext}\sin(\theta_u) - b_{u,ext}\cos(\theta_u))}. \quad (31)$$

It follows from (27) that

$$f(C, \xi; u_0) = (1 - (g(\xi; u_0)/4)), \quad (32)$$

and so, $\hat{\xi}$ in (31) also maximizes $f(C, \xi; u_0)$ with $\hat{f}(C; u_0) = f(C, \hat{\xi}; u_0)$.

Using similar arguments, the value of ξ that minimizes the function g in (30) for a delta (from (29)) is given by

$$\tan 3\hat{\xi} = \frac{\sum_{u \in \mathcal{W}_{u_0}} (b_{u,ext}\sin(\theta_u) - a_{u,ext}\cos(\theta_u))}{\sum_{u \in \mathcal{W}_{u_0}} (a_{u,ext}\sin(\theta_u) + b_{u,ext}\cos(\theta_u))}, \quad (33)$$

and we have $\hat{f}(D; u_0) = f(D, \hat{\xi}; u_0)$.

ACKNOWLEDGMENTS

REFERENCES

[1] E. R. Henry, *Classification and Uses of Fingerprints*. London: Routledge, 1900.
[2] A. M. Bazen and S. H. Gerez, "Systematic methods for the computation of the directional fields and singular points of fingerprints," *IEEE Trans. PAMI*, vol. 24, no. 7, pp. 905–919, 2002.
[3] C. L. Wilson, G. T. Candela, and C. I. Watson, "Neural network fingerprint classifiaction," *J. Artificial Neural Networks*, vol. 2, pp. 203–228, 1994.
[4] L. O'Gorman and J. V. Nickerson, "An approach to fingerprint filter design," *Pattern Recognition*, vol. 22, no. 1, pp. 362–385, 1987.
[5] A. R. Rao, *A Taxonomy For Texture Description and Identification*. Springer-Verlag, New York, 1990.
[6] L. Hong, Y. Wan, and A. K. Jain, "Fingerprint image enhancement: Algorithm and performance evaluation," *IEEE Trans. PAMI*, vol. 20, no. 8, pp. 777–789, 1998.
[7] A. K. Jain, L. Hong, S. Pankanti, and R. Bolle, "An identity authetication system using fingerprints," *IEEE Trans. PAMI*, vol. 85, no. 9, pp. 1365–1388, 1997.
[8] N. K. Ratha, S. Chen, and A. K. Jain, "Adaptive flow orientation based feature extraction in fingerprint images," *Pattern Recognition*, vol. 28, pp. 1657–1672, 1995.
[9] O. Nakamura, K. Goto, and T. Minami, "Fingerprint classification by directional distribution patterns," *Systems, Computers, Controls*, vol. 13, no. 5, pp. 81–89, 1982.
[10] V. S. Srinivasan and N. N. Murthy, "Detection of singular points in fingerprint images," *Pattern Recognition*, vol. 25, no. 2, pp. 139–153, 1992.
[11] A. R. Rao and R. C. Jain, "Computerized flow field analysis: Oriented texture fields," *IEEE Trans. Pattern Analysis and Machine Intelligence*, vol. 14, no. 7, pp. 693–709, 1992.
[12] P. Perona, "Orientation diffusions," *IEEE Trans. Image Processing*, vol. 7, no. 3, pp. 457–467, 1998.
[13] A. K. Jain, S. Prabhakar, L. Hong, and S. Pankanti, "Filterbank-based fingerprint matching," *IEEE Trans. Image Processing*, vol. 9, no. 5, pp. 846–859, 2000.
[14] D. Geman and S. Geman, "Stochastic relaxation, Gibbs distribution and the Bayesian restoration of images," *IEEE Trans. on PAMI*, vol. 6, no. 6, pp. 721–741, 1984.
[15] T. Simchony, R. Chellappa, and Z. Lichtenstein, "Relaxation algorithms for map estimation gray-level images with multiplicative noise," *IEEE Trans. on Information Theory*, vol. 36, no. 3, pp. 608–613, 1990.
[16] J. L. Marroquin, S. Mitter, and T. Poggio, "Probabilistic solution of ill-posed problems in computational vision," *Journal of the American Statistical Association*, vol. 82, no. 397, pp. 76–89, 1987.
[17] M. L. Comer and E. J. Delp, "Parameter estimation and segmentation of noisy or textured images using the EM algorithm and mpm estimation," *Proc. of IEEE Int. Conf. on Image Proc.*, vol. 2, pp. 650–654, 1994.
[18] J. Zhang, J. W. Modestino, and D. A. Langan, "Maximum likelihood parameter estimation for unsupervised stochastic model-based image segmentation," *IEEE Trans. on Image Processing*, vol. 2, no. 4, pp. 404–420, 1994.
[19] H. Derin and W. Cole, "Segmentation of textured images, using Gibbs random fields," *Comput. Vision Graphics and Image Process.*, vol. 32, pp. 72–98, 1986.
[20] Y. Zhang, M. Brady, and S. Smith, "Segmentation of brain mr images through a hidden Markov random field model and the EM algorithm," *IEEE Trans. on Medical Imaging*, vol. 20, no. 1, pp. 45–57, 2001.
[21] D. Geman, S. Geman, C. Graffigne, and P. Dong, "Boundary detection by constrained optimization," *IEEE Trans. on PAMI*, vol. 12, no. 7, pp. 609–628, 1990.
[22] D. Geman and G. Reynolds, "Constrained restoration and the recovery of discontinuities," *IEEE Trans. on PAMI*, vol. 14, no. 3, pp. 767–783, 1992.
[23] P. Green, "Bayesian reconstructions from emission tomography data using a modified EM algorithm," *IEEE Trans. on Medical Imaging*, vol. 9, no. 1, pp. 84–93, 1990.
[24] S. Geman and S. McClure, "Statistical methods for tomographic image reconstruction," *Bull. Int. Stat. Inst.*, vol. 4, pp. 5–21, 1987.
[25] S. Z. Li, *Markov random field modeling in image analysis*. Springer, Tokyo, 2001.
[26] R. Chellappa and A. Jain, Eds., *Markov random fields: Theory and Applications*. Academic Press, 1993.
[27] S. T. Acton and A. C. Bovik, "Nonlinear image estimation using piecewise and local image models," *IEEE Transactions on Image Processing*, vol. 7, no. 7, pp. 979–991, 1998.
[28] ——, "Piecewise and local image models for regularized image restoration using cross-validation," *IEEE Transactions on Image Processing*, vol. 8, no. 5, pp. 652–665, 1999.
[29] J. E. Besag, "Spatial interaction and the statistical analysis of lattice systems (with discussions)," *J. R. Stat. Soc. Ser. B Stat. Methodol.*, vol. 36, pp. 192–236, 1974.
[30] ——, "Statistical analysis of non-lattice data," *The Statistician*, vol. 24, pp. 179–195, 1975.
[31] K. Lange, D. R. Hunter, and I. Yang, "Optimization transfer using surrogate objective functions (with discussion)," *Journal of Computational and Graphical Statistics*, vol. 9, pp. 1–59, 2000.
[32] "NIST: 8-bit gray scale images of fingerprint image groups (FIGS)," online: http://www.nist.gov/srd/nistsd4.htm.

Sarat C. Dass received the MSc degree and the PhD degree in Statistics from Purdue University, USA, in 1995 and 1998, respectively. He worked as a visiting Assistant Professor (in the period 1998-2000) at the Department of Statistics, University of Michigan. Starting 2000, he joined the Department of Statistics & Probability at Michigan State University. His research and teaching interests include statistical image processing and pattern recognition, shape analysis, spatial statistics, Bayesian computational methods, foundations of Statistics and non-parametric statistical methods. He has been actively collaborating with computer scientists in several pattern recognition and image processing problems.